



Optimization and batch studies on adsorption of malachite green dye using rambutan seed activated carbon

Mohd Azmier Ahmad^a, Nur Syahidah Afandi^a, Kayode Adesina Adegoke^b,
Olugbenga Solomon Bello^{a,b,*}

^aSchool of Chemical Engineering, Engineering Campus, Universiti Sains Malaysia, 14300 Nibong Tebal, Penang, Malaysia, emails: chazmier@usm.my (M.A. Ahmad), nsafandi@usm.my (N.S. Afandi), osbello06@gmail.com (O.S. Bello)

^bDepartment of Pure and Applied Chemistry, Ladoko Akintola University of Technology, P.M.B 4000, Ogbomoso, Oyo State, Nigeria, email: kwahyourday@gmail.com (K.A. Adegoke)

Received 11 April 2015; Accepted 21 October 2015

ABSTRACT

Rambutan seeds (*Nephelium lappaceum* L.)-based activated carbon (RSAC) was prepared using potassium hydroxide (KOH) activation and carbon dioxide (CO₂) gasification methods. The adsorbent prepared was characterized using Fourier transform infrared, SEM, proximate analysis, and BET techniques, respectively. The effects of three variable parameters; activation temperature, activation time, and chemical impregnation ratio (IR) (KOH: char by weight) on the preparation of RSAC used for the removal of MG dye was investigated. Based on the central composite design, quadratic and two factor interaction (2FI) models were, respectively, employed to correlate the effect of variable parameters on the preparation of RSAC used for the percentage MG dye removal and activated carbon yield. From the analysis of variance, the most influential factor on each experimental design response was identified. The optimum conditions of MG dye removal by RSAC are: activation temperature (802°C), activation time (1.0 h), and IR (2.4), respectively. The percentage MG dye removal obtained was 91.45% resulting in 22.56% RSAC yield. The percentage error between predicted and experimental results for the removal of MG dye is 2.4%. The effects of operational parameters like pH, initial dye concentration, contact time, and solution temperature were investigated using batch method. Graphical correlations of eight different adsorption isotherm models were carried out. Freundlich isotherm fitted the adsorption data most. The data were also analyzed by the Lagergren pseudo-first-order, Ho Mc Kay pseudo-second-order, Elovich and Avrami kinetic models. Pseudo-second-order kinetic model best represents the kinetic data and the mechanism of adsorption was controlled by both film and intraparticle diffusions. Thermodynamic studies gave negative ΔG° values, indicating that the process of MG dye adsorption onto RSAC was spontaneous. The positive values of ΔH° and ΔS° suggest that the process of dye adsorption was endothermic.

Keywords: Rambutan seeds; Malachite green; Central composite design; Kinetics

*Corresponding author.

1. Introduction

Today, many dyes are used in different industries which discharge large volumes of wastewater. The wastewater contains large amount of dissolved dye-stuff and other products. The disposal of dye laden wastewater is a big challenge; it causes severe harm to the aquatic environment [1,2]. Some of the dyes present in wastewater even decompose into carcinogenic aromatic amines under anaerobic conditions and cause serious health problems to human beings as well as other animals. Dyes have long been used in dyeing, paper and pulp, textile, plastic, leather, cosmetic, and food industries. Effluents discharged from these industries pose certain hazards and environmental problems. Wastewater from these industries may present an eco-toxic hazard and introduce the potential danger of bioaccumulation, which may eventually affect human beings [3]. There are various conventional methods of removing dyes from wastewaters. Among these methods, adsorption is the most versatile and widely used method because of its low cost and ease of operation [4,5]. A number of agricultural wastes and by-products of cellulose origin have been studied for their abilities to remove dyes from aqueous solutions [6] such as peanut hulls [7], maize bran [8], sawdust [9], clay sugar beet pulp [10], crab peel [11], granular kohlrabi peel [12], raw barley straw [13], eggshell [14], aquaculture shell powders [15], etc. Activated carbon is regarded as one of the most effective materials for the removal of dyes [16] but due to its high cost and 10–15% loss during regeneration, unconventional adsorbents like wood [17], silica, [18], clay and activated clay [19,20], agricultural residues [21], etc. have attracted the attention of several investigations for the removal of dyes.

Malachite green is a triphenyl methane dye used for coloring cotton, wool, silk, paper, leather, etc. It is also used as parasiticide, fungicide, antiprotozoan, and antibacterial agent [22]. This dye is recommended for only external applications, its oral consumption is toxic, hazardous, and carcinogenic due to presence of nitrogen [23]. It is known to be highly toxic to mammalian cells and acts as a tumor-enhancing agent. It decreases food intake, growth, and fertility rates, causes damage to liver, spleen, kidney, and heart, inflicts lesions on skin, eyes, lungs, and bones. Hence, it is important to remove it from effluent discharge. Rambutan (*Nephelium lappaceum* L.) is a popular tropical fruit which belongs to *Sapindaceae* family [24]. In Malaysia, a rambutan tree may produce approximately 5,000–6,000 rambutan fruits with total weight of 60–70 kg. There are products related to rambutan such as jams, marmalade, spread, jelly, and canned

foods. However, due to the high consumption of rambutan's edible part, massive amount of the seed are disposed, causing severe problem in the community as they gradually ferment and release offensive odors. Therefore, conversion of rambutan seed into activated carbon would provide a potentially cheap alternative precursor and reduce the cost of waste disposal as well [25].

The response surface methodology (RSM) is an efficient statistical technique for optimization of multiple variables to predict the best performance conditions with minimum number of experiments [17]. Central composite design (CCD) involves the following steps: performing the statistically designed experiments according to the design, factors, and levels selected; estimating the coefficients of the mathematical model to predict the response and check its adequacy [18,19].

The aim of the present study is to optimize the removal of the triphenylmethane dye (MG) using rambutan seeds. RSM was used to study the effects of three activated carbon preparation variables (CO_2 activation temperature, CO_2 activation time, and impregnation ratio (IR)) on two responses. Empirical models correlating MG dye removal and the activated carbon yield with the three variables were then developed. The RS-based activated carbon prepared under optimum conditions was further characterized to determine its physical and chemical characteristics. In this study, rambutan seed-based activated carbon (RSAC) was prepared by physiochemical activation and tested for its ability to remove MG dye from aqueous solution. The equilibrium and kinetic data of the adsorption process were then analyzed to study the adsorption isotherms, kinetics, thermodynamics, and mechanism of MG dye adsorption on RSAC.

2. Materials and methods

2.1. Preparation of activated carbon

2.1.1. Activated carbon preparation

Rambutan seeds (RS) were purchased from a local market in Parit Buntar area, Perak, Malaysia. The seeds were cleaned and rinsed thoroughly with distilled water. It was then dried to constant weight and stored in an air tight container for further use. 100 g of rambutan seed was placed in a vertical tubular reactor. Nitrogen gas was purged into the reactor to create inert condition. The flow rate of nitrogen gas and the heating rate were held at $150 \text{ cm}^3/\text{min}$ and $10^\circ\text{C}/\text{min}$, respectively. The temperature was ramped from room temperature to 700°C and held for 1 h.

Then, the reactor was cooled down to room temperature. The char produced was stored in air-tight container for further treatment. The char produced was then impregnated. The IR was calculated using:

$$IR = \frac{w_c}{w_0} \quad (1)$$

where w_{KOH} is the dry weight (g) of potassium hydroxide pellet and w_{char} is the dry weight (g) of char. The char and KOH powder (depending on the IR) were mixed together with deionized water in a 250 ml beaker. The mixture was stirred thoroughly until it dried in an oven overnight at 105°C for dehydrating purpose. The KOH impregnated char was placed inside the vertical tubular reactor for activation process. The system was purged under nitrogen flow of 150 cm³/min. The temperature was ramped from ambient temperature to the activation temperature at heating rate of 10°C/min. Once the desired activation temperature was reached, the gas flow was switched to carbon dioxide at flow rate of 150 cm³/min to complete the activation process. Then, the reactor was cooled to room temperature under nitrogen flow. The sample was washed with 0.1 M HCl. It was further washed with deionized water several times until the pH of the washing solution reached 6.5–7. The pH was measured using pH meter (Model Delta 320, Mettler Toledo, China). Filter paper and filter funnel were used in the washing process. The washed sample was kept in an oven at 105°C for 12 h. The dried sample which was the activated carbon (RSAC) was stored in air-tight containers for further characterization and adsorption studies. The RSAC yield was calculated using the equation:

$$\text{Yield (\%)} = \frac{w_{\text{KOH}}}{w_{\text{char}}} \times 100 \quad (2)$$

where w_c and w_0 are the dry weight of RSAC (g) and the dry weight of precursor (g), respectively.

2.1.2. Adsorbate used

Malachite green (MG) was used as adsorbate to determine the adsorption performance of the prepared activated carbon. The properties of MG dye used are listed in Table 1.

2.1.3. Adsorption studies

For batch adsorption studies, 0.2 g of RSAC were mixed with 100 ml aqueous dye solution of 100 mg/L

initial concentration in 20 sets of 250-ml Erlenmeyer flasks. The mixture was agitated at 120 rpm at 30°C until equilibrium was reached. The concentration of MG dye solution was determined using a UV-vis spectrophotometer (UV-1800 Shimadzu, Japan) at a maximum wavelength of 618 nm. The percentage dye removal at equilibrium was calculated using Eq. (3):

$$\text{Removal (\%)} = \frac{C_o - C_e}{C_o} \times 100 \quad (3)$$

where C_o and C_e are the liquid-phase dye concentrations at initial and equilibrium states (mg/L), respectively.

2.1.4. Experimental design using CCD

A standard RSM design called a CCD was used to study the parameter for AC preparation. In this work, three independent variables studied for the AC preparation are: x_1 , Activation temperature (°C), x_2 , Activation time (h) and x_3 , KOH: char IR. The ranges and the levels of the variables investigated are given in Table 2. Based on the ranges and the levels given, a complete design matrix of the experiments was employed as shown in Table 3. There are 8 factorial points, 6 axial points and 6 replicates at the center points, indicated by a total of 20 experiments for each precursor, as calculated from Eq. (4):

$$N = 2^n + 2n + n = 2^3 + 2 \times 3 + 6 = 20 \quad (4)$$

where N is the total number of experiments required and n is the number of variables. The center points were used to verify the reproducibility of the data and the experimental error. The variables were coded to the (-1, 1) interval where low and high level were coded as -1 and +1, respectively. The axial points are located at $(\pm a, 0, 0)$, $(0, \pm a, 0)$, and $(0, 0, \pm a)$ where a is the distance of the axial point from center and makes the design rotatable. In this study, a value was fixed at 1.682 (rotatable). The two responses are MG removal (Y_1) and AC yield (Y_2). Each response was used to develop an empirical model which correlated the response to the variables using a second-degree polynomial equation as follow [26]:

$$Y = b_0 + \sum_{i=1}^n b_i x_i + \left(\sum_{i=1}^n b_{ii} x_i \right)^2 + \sum_{i=1}^{n-1} \sum_{j=i+1}^n b_{ij} x_i x_j \quad (5)$$

Table 1
Properties of malachite green dye

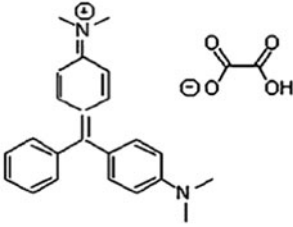
Properties	
Chemical name	4-[(4-dimethylaminophenyl)-phenyl-methyl]-N,N-dimethyl-aniline
Common name	Malachite green hydrochloride
Generic name	Basic green 4
CAS number	123333-61-9
Color index number	42,000
Ionization	Basic
Maximum wavelength	618 nm
Empirical formula	C ₂₃ H ₂₆ N ₂ O·HCl
Molecular weight	382.93 g/mol
Chemical structure	

Table 2
Independent variables and their coded levels for the CCD

Variables (factors)	Code	Units	Coded variables level				
			- α	-1	0	+1	+ α
Activation temperature	x_1	°C	649	700	775	850	901
Activation time	x_2	h	0.32	1.00	2.00	3.00	3.68
IR	x_3		0.15	1.00	2.25	3.50	4.35

where Y is the predicted response, b_0 the constant coefficient, b_i the linear coefficients, b_{ij} the interaction coefficients, b_{ii} the quadratic coefficients, and x_i, x_j are the coded values of the AC preparation variables. The coefficient with one factor represents the effect of particular factor, while the coefficient with two factors and those with second-order terms represent the interaction between two factors and quadratic effects. In order to strike a compromise between the responses, the function of desirability was applied by using Design Expert software version 7.1.5 (STAT-EASE Inc., Minneapolis, USA). The "Prob. > F " value of less than 0.05 indicates that the model is significant [27]. It is desirable to indicate the influence of particular model terms that have significant effects on the response. Experimental conditions with the highest desirability were selected to be verified.

2.1.5. Characterization of RSAC

The surface area, pore volume, and average pore diameter of the RSAC were determined using the

nitrogen adsorption isotherm. The surface area of the sample was determined using Brunauer–Emmett–Teller (BET). The surface morphology of the sample was examined using a scanning electron microscope (JEOL, JSM-6460 LV, Japan). Proximate analysis was carried out using thermo gravimetric analyser (Perkin–Elmer TGA7, USA) and Fourier transform infrared (FTIR) analysis was performed to determine the functional groups responsible for the adsorption of MG dye on RSAC.

2.1.6. Batch equilibrium studies

The effects of initial dye concentration, contact time, solution temperature, and solution pH on the adsorption uptake of MG dye on RSAC were studied. Sample solutions were withdrawn at intervals to determine the residual concentration by using UV–vis spectrophotometer at the maximum wavelength of 618 nm. The amount of dye adsorbed at equilibrium, q_e (mg/g) was calculated as:

Table 3
Experimental design matrixes for RSAC preparation

Run	AC preparation variables		
	Activation temperature, x_1 (°C)	Activation time, x_2 (h)	IR, x_3
1	700(−1)	1.00(−1)	1.00(−1)
2	850(+1)	1.00(−1)	1.00(−1)
3	700(−1)	3.00(+1)	1.00(−1)
4	850(+1)	3.00(+1)	1.00(−1)
5	700(−1)	1.00(−1)	3.50(+1)
6	850(+1)	1.00(−1)	3.50(+1)
7	700(−1)	3.00(+1)	3.50(+1)
8	850(+1)	3.00(+1)	3.50(+1)
9	649(−1.682)	2.00(0)	2.25(0)
10	901(+1.682)	2.00(0)	2.25(0)
11	775(0)	0.32(−1.682)	2.25(0)
12	775(0)	3.68(+1.682)	2.25(0)
13	775(0)	2.00(0)	0.15(−1.682)
14	775(0)	2.00(0)	4.36(+1.682)
15	775(0)	2.00(0)	2.25(0)
16	775(0)	2.00(0)	2.25(0)
17	775(0)	2.00(0)	2.25(0)
18	775(0)	2.00(0)	2.25(0)
19	775(0)	2.00(0)	2.25(0)
20	775(0)	2.00(0)	2.25(0)

$$q_e = \frac{(C_o - C_e)V}{W} \quad (6)$$

where C_o and C_e (mg/L) are the liquid-phase concentrations at initial and at equilibrium, respectively. V is the volume of the solution (dm^3) and W is the mass (g) of RSAC used.

2.1.7. Effect of initial adsorbate concentration and contact time

100 ml of MG dye solution with known initial concentration was placed in a series of 250 ml Erlenmeyer flasks. The amount of adsorbent that was added into each flask was fixed at 0.1 g. The flasks were placed in an isothermal water bath shaker (Model Protech, Malaysia) at constant temperature of 30°C, with rotation speed of 120 rpm, until equilibrium point was reached. Samples are withdrawn at intervals to determine the residual concentration of the dye at 618 nm wavelength using a UV–vis Spectrophotometer.

2.1.8. Effect of solution temperature

The effect of solution temperature on the adsorption process was carried out by varying the adsorption temperature at 30, 45, and 60°C by adjust-

ing the temperature controller of the water bath shaker, while other operating parameters such as adsorbent dosage (0.1 g) and rotation speed (120 rpm) were kept constant.

2.1.9. Effect of solution pH

Solution pH was studied by varying the initial pH of solution from 2 to 12. The pH was adjusted by 0.1 M NaOH or 0.1 M HCl and measured by using a pH meter. The adsorbent dosage, rotation speed, solution temperature, and initial dye concentration were fixed at 0.1 g, 120 rpm, 30°C, and 100 mg/L, respectively.

2.1.10. Adsorption isotherm studies

This was carried out by fitting the equilibrium data to Langmuir, Freundlich, Temkin, Dubinin–Radushkevich, Sips, Vieth–Sladek, Bruoers–Sotolongo, and Radke–Prausnitz isotherms. The applicability and suitability of the isotherm equations to the equilibrium data were compared by judging the values of the correlation coefficients, R^2 and normalized standard deviation, Δq_e . Linear regression was carried out by using Microsoft Excel spreadsheet with Solver add-in to determine the isotherm parameters.

2.1.11. Langmuir isotherm

This model depends on the assumption that intermolecular forces decrease rapidly with distance and consequently help to predict the existence of monolayer coverage of the adsorbate on the outer surface of adsorbent. The linear form of Langmuir isotherm equation [28] is given by:

$$\frac{C_e}{q_e} = \frac{1}{Q_0 k_L} + \frac{1}{Q_0} C_e \quad (7)$$

where C_e is the equilibrium concentration of the adsorbate (mg/L), q_e is the amount of adsorbate adsorbed per unit mass of adsorbent (mg/g), Q_0 is the maximum monolayer adsorption capacity of the adsorbent (mg/g), and k_L is the Langmuir adsorption constant related to the free energy of adsorption (L/mg). The constant values are evaluated from intercept and slope of the linear plot of experimental data of (C_e/q_e) vs. C_e . The essential characteristics of Langmuir equation can be expressed in terms of dimensionless separation factor, R_L , defined as:

$$R_L = \frac{1}{(1 + k_L C_0)} \quad (8)$$

where C_0 is the highest initial dye concentration whereas R_L value implies the adsorption is unfavorable ($R_L > 1$), linear ($R_L = 1$), favorable ($0 < R_L < 1$), or irreversible ($R_L = 0$).

2.1.12. Freundlich isotherm

The Freundlich model is an empirical equation based on adsorption of heterogeneous surface or surface supporting sites of varied affinities. It is assumed that the stronger binding sites are occupied first and that the binding strength decreases with the increasing degree of site occupation. The Freundlich isotherm [29] is expressed as:

$$\log q_e = \log k_F + (1/n) \log C_e \quad (9)$$

where q_e is amount of adsorbate adsorbed per unit mass of adsorbent (mg/g); k_F is Freundlich isotherm constant (mg/g) (L/mg) $^{1/n}$; which indicate the relative adsorption capacity of the adsorbent related to the bonding energy; C_e is equilibrium concentration of the adsorbate (mg/L) and n_F is the heterogeneity factor representing the deviation from linearity of adsorption and is also known as Freundlich coefficient.

If the plot of $(\log q_e)$ against $(\log C_e)$ gave straight line, it indicates that the Freundlich isotherm fit the adsorption data. Other constants can be calculated from the slope ($1/n$) and intercept ($\log k_F$) of the linear plot of experimental data. The slope of $1/n$ ranging between 0 and 1 is a measure of adsorption intensity, becoming more heterogeneous as its value gets closer to zero.

2.1.13. Temkin isotherm

Temkin isotherm contains a factor that explicitly takes into account the adsorbent–adsorbate interactions. This model assumes that the heat of adsorption of all the molecules in the layer would decrease linearly with coverage due to adsorbent–adsorbate interactions. The Temkin model [30] is expressed as:

$$q_e = B \ln A_T + B \ln C_e \quad (10)$$

where B is RT/b constant related to the heat of adsorption (L/mg); q_e is amount of adsorbate adsorbed at equilibrium (mg/g); C_e is equilibrium concentration of adsorbate (mg/L); T is absolute temperature; R is universal gas constant (8.314 J/mol K) and A_T is equilibrium binding constant (L/mg). A graph of plot of q_e vs. $\ln C_e$ will yield both value of slope, B and intercept, A_T .

2.1.14. Dubinin–Radushkevich isotherm

Dubinin–Radushkevich isotherm is an empirical model initially for the adsorption of subcritical vapors onto micropore solids following a pore filling mechanism. It is applied to distinguish the physical and chemical adsorption for removing a molecule from its location in the sorption space to the infinity, which can be express as [31]:

$$q_e = q_s \exp(-B_{DR} \varepsilon^2) \quad (11)$$

where ε can be correlated:

$$\varepsilon = RT \ln \left[1 + \frac{1}{C_e} \right] \quad (11a)$$

$$E = \frac{1}{\sqrt{2B_{DR}}} \quad (11b)$$

where R , T , and C_e represent the gas constant (8.314 J/mol K), absolute temperature (K), and

adsorbate equilibrium concentration (mg/L), respectively. The value of B_{DR} was then used to estimate free energy E of sorption per molecule of the sorbate when it is transferred to the surface of the solid from infinity in the solution. A plot of $\ln q_e$ vs. e^2 will yield a straight line where B_{DR} and q_s are obtained from the slope and intercept.

2.1.15. Sips isotherm

Sips isotherm model is a combined form of Langmuir and Freundlich expressions deduced for predicting the heterogeneous adsorption systems and circumventing the limitation of the rising adsorbate concentration associated with Freundlich isotherm model [32]. At high adsorbate concentration, it predicts monolayer adsorption characteristics of Langmuir, while in low adsorbate concentration; it reduces to Freundlich isotherm. The Sips model expressed as:

$$q_e = \frac{q_m(k_s C_e)^{m_s}}{1 + (k_s C_e)^{m_s}} \quad (12)$$

where k_s is Sips isotherm model constant and m_s is Sips' isotherm model exponent.

2.1.16. Vieth–Sladek isotherm

The Vieth–Sladek isotherm is given by the following equation [33]:

$$q_e = k_{vs} C_e + \frac{q_m B_{vs} C_e}{1 + B_{vs} C_e} \quad (13)$$

where q_e is the adsorbed amount at equilibrium (mg/g); C_e is the adsorbate equilibrium concentration (mg/L); q_m is maximum adsorption capacity, k_{vs} and B_{vs} are Vieth–Sladek constants. The Vieth–Sladek isotherm is used for estimating diffusion rates in solid materials from transient sorption.

2.1.17. Brouers–Sotolongo isotherm

The Brouers–Sotolongo model [34] is expressed as:

$$q_e = q_m(1 - \exp(-k_{BS}(C_e)^{\alpha_{BS}})) \quad (14)$$

where k_{BS} and α_{BS} are Brouers–Sotolongo constants. The exponent is a measure of the width of the sorption energy distribution and energy heterogeneity of the sorbent surface.

2.1.18. Radke–Prausnitz isotherm

The Radke–Prausnitz model [35] isotherm can be represented as:

$$q_e = \frac{k_{RP} q_m C_e}{(1 + k_{RP} C_e)^{m_{RP}}} \quad (15)$$

where q_e is the adsorbed amount at equilibrium (mg/g), q_{mRP} is the Radke–Prausnitz maximum adsorption capacity (mg/g), C_e is the adsorbate equilibrium concentration (mg/L), k_{RP} is the Radke–Prausnitz equilibrium constant, and m_{RP} is the Radke–Prausnitz model exponent. Radke–Prausnitz model will be converted to another model under certain conditions. At low concentration, if the value of exponent's m_{RP} is equal to unity, the model of Radke–Prausnitz is reduced to the Langmuir model. While, if liquid phase concentration is high, the model of Radke–Prausnitz is converted to the Freundlich.

2.2. Batch kinetic studies

This procedure is similar to that of batch equilibrium studies. The difference is that the absorbent–adsorbate solution was taken at preset time intervals and the concentration of the solution was measured. The amount of adsorption at time t , q_t (mg/g), was calculated using Eq. (16):

$$q_t = \frac{(C_o - C_t)V}{W} \quad (16)$$

where C_o and C_t (mg/L) are the liquid-phase concentrations of adsorbate at initial and at any time t , respectively. V is the volume of the solution and W is the mass of adsorbent used. The adsorption kinetics of dye on adsorbent was investigated using pseudo-first-order model, pseudo-second-order model, Avrami, and Elovich models respectively.

2.2.1. Pseudo-first-order kinetic model

The pseudo-first-order kinetic model equation is generally expressed as follows [36]:

$$\ln(q_e - q_t) = \ln q_e - k_1 t \quad (17)$$

where q_e is the amount of adsorbate adsorbed at equilibrium, (mg/g), q_t is the amount of solute adsorb per unit weight of adsorbent at time t , (mg/g), k_1 is the rate constant of pseudo-first-order sorption (1/h). A plot of $\ln(q_e - q_t)$ vs. t gives a straight line with slope of k_1 and intercept of $\ln q_e$.

2.2.2. Pseudo-second-order kinetic model

The pseudo-second-order equation can be expressed as [37]:

$$\frac{t}{q_t} = \frac{1}{k_2 q_e^2} + \frac{1}{q_e} t \quad (18)$$

The constant k_2 is used to calculate the initial sorption rate, h , at $t = 0$, as follows:

$$h = k_2 q_e^2 \quad (18a)$$

Thus the rate constant k_2 , initial adsorption rate h and predicted q_e can be calculated. The linear plot of t/q_e vs. t gives $1/q_e$ as the slope and $1/h$ as the intercept.

2.2.3. Elovich kinetic model

The simplified Elovich equation is expressed as [38]:

$$q_t = \frac{1}{\beta} \ln(\alpha\beta) + \frac{1}{\beta} \ln t \quad (19)$$

where α is the initial desorption rate (mg/(g min)) and β is the desorption constant (g/mg) during the experiment. Plot of q_t vs. $\ln t$ gave a linear relationship with slope of $1/\beta$ and an intercept of $(1/\beta) \ln(\alpha\beta)$. The $1/\beta$ value reflects the number of sites available for adsorption whereas the value of $1/\beta \ln(\alpha\beta)$ indicates the adsorption quantity when $\ln t$ equal to zero.

2.2.4. Avrami kinetic model

The Avrami equation is used to verify specific changes of kinetic parameters as functions of temperature and reaction time. It is also an adaptation of kinetic thermal decomposition modeling [39].

The Avrami kinetic model is expressed as:

$$\ln(-\ln(1 - \alpha)) = n \ln k_{AV} + n \ln t \quad (20)$$

where α is the adsorption fraction at time t , k_{AV} is the adjusted kinetic constant, and n_{AV} is another constant, which is related to the adsorption mechanism. n value can be used to verify possible interactions of the adsorption mechanism in relation to the contact time and the temperature.

2.2.5. Validity of kinetic model

The applicability and fitting of the isotherm equation to the kinetic data was compared by judging from

the R^2 values and the normalized standard deviation Δq_t (%) calculated from Eq. (21). The normalized standard deviation, Δq_t (%) was used to verify the kinetic models used to describe the adsorption process. It is expressed as:

$$\Delta q_t (\%) = \frac{100 \sqrt{\sum_T^n [(q_{\text{exp}} - q_{\text{cal}})/q_{\text{exp}}]^2}}{n - 1} \quad (21)$$

where n is the number of data points, q_{exp} and q_{cal} (mg/g) are the experimental and calculated adsorption capacity values. Lower value of Δq_t indicates good fit between experimental and calculated data.

2.3. Adsorption thermodynamics

The experimental data obtained from batch adsorption studies performed earlier were analyzed by using the thermodynamic equations as expressed by Eq. (22):

$$\Delta G = -RT \ln k_L \quad (22)$$

$$\ln k = \frac{\Delta S}{R} - \frac{\Delta H}{RT} \quad (22a)$$

ΔG was calculated using Eq. (22). The values of ΔH and ΔS can be obtained, respectively, from the slope and intercept of Van't Hoff plot of $\ln k_L$ vs. $1/T$ (Eq. (22a)). Values of k_L may be calculated from the relation $\ln q_e/C_e$ at different solution temperatures. Arrhenius equation has been applied to evaluate the activation energy of adsorption representing the minimum energy that reactants must have for the reaction to proceed, as shown by the following relationship:

$$\ln k_2 = \ln A - \frac{E_a}{RT} \quad (22c)$$

where k_2 is the rate constant obtained from the pseudo-second-order kinetic model, (g/mg h), E_a is the Arrhenius activation energy of adsorption, (kJ/mol), A is the Arrhenius factor, R is the universal gas constant (8.314 J/mol K), and T is the absolute temperature. When $\ln k_2$ is plotted against $1/T$, a straight line with slope of $-E_a/R$ is obtained.

2.4. Adsorption mechanism

The adsorption mechanisms of MG dye on the adsorbent were investigated using intraparticle diffusion model represented by Eq. (23). The applicability

and fitting of the model throws more light into the mechanism of MG dye adsorption onto RSAC prepared.

2.4.1. Intraparticle diffusion model

Intraparticle diffusion model [40] is expressed as shown in Eq. (23):

$$q_t = k_{pi}t^{1/2} \quad (23)$$

where C_i is the intercept and k_{pi} ($\text{mg/g h}^{1/2}$) is the intraparticle diffusion rate constant, which can be evaluated from the slope of the linear plot of q_t vs. $t^{1/2}$. The q_t is the amount of solute adsorbed per unit weight of adsorbent per time, (mg/g), and $t^{1/2}$ is the half adsorption time, (g/h mg). The intercept of the plot reflects the boundary layer effect. The larger the intercept, the greater the contribution of the surface sorption in the rate-controlling step. If the regression of q_t vs. $t^{1/2}$ is linear, and passes through the origin, then intraparticle diffusion is the sole rate-limiting step. If the linear plots at each concentration did not pass through the origin, it indicates that the intraparticle diffusion was not only rate controlling step [41].

3. Results and discussion

3.1. Model fitting and statistical analysis

Design Expert Software version 7.1.5.1 (STAT-EASE Inc., Minneapolis, US) was used to analyze the experimental data.

3.2. Development of regression model equation

In this study, we selected CCD for the optimization of MG dye removal by RSAC. The three significant variables can be approximated by the quadratic model equation which is shown below. As suggested by the software, dye removal response (Y_1), and carbon yield (Y_2), the quadratic and 2FI models were selected. The R^2 values for Eqs. (24) and (25) were, respectively, 0.9900 and 0.8949 as shown in Figs. 1 and 2. The R^2 value shows good agreement between experimental and predicted data as shown in Figs. 1 and 2 with the model prediction suggested in Eqs. (24) and (25). R^2 value closer to unity indicates the suitability of the model equation. In fact, a smaller standard deviation indicated closeness of predicted value to the experimental value for the response. The empirical formula models in terms of coded factors are represented as:

$$Y_1 = 91.11 + 4.52x_1 + 0.63x_2 + 6.09x_3 - 0.63x_1^2 - 1.19x_2^2 - 0.26x_3^2 - 3.56x_1x_2 - 1.00x_1x_3 - 3.92x_2x_3 \quad (24)$$

$$Y_2 = 21.34 - 1.54x_1 - 1.25x_2 - 1.17x_3 - 0.12x_1x_2 - 0.004x_1x_3 + 0.55x_2x_3 \quad (25)$$

3.3. Preparation of RSAC using design of experiment

The complete design matrix for preparation variables of RSAC and responses are given in Table 4. Three variables studied were; activation temperature (x_1), activation time (x_2), and KOH/char IR (x_3) with two responses; MG dye removal (Y_1) and RSAC yield (Y_2). MG dye removal was found to range from 69.89 to 92.54%, whereas the RSAC yield obtained ranged from 16.73 to 26.82% (Table 4). The analysis of variance (ANOVA) was carried out to determine the adequacy of the model developed. Tables 5 and 6 show the ANOVA analysis for MG dye removal by RSAC, as well as RSAC yield. From Table 5, the model F -value of 110.33 and Prob. $> F$ of less than 0.0001 indicated that the model was significant. The value of model terms Prob. $> F$ less than 0.05 indicates that the model terms are significant. For MG dye adsorption, x_1 , x_3 , x_1^2 , x_2^2 , x_3^2 , and x_1x_3 were found significant, whereas x_2 , x_1x_3 and x_2x_3 were insignificant model terms to the response. Table 6 shows the 2FI model of RSAC yield. The model F -value of 18.45 with Prob. $> F$ of 0.0001 indicates that RSAC yield model was significant. For RSAC yield, x_1 , x_2 , x_3 , and x_1x_2 were significant models term whereas x_1x_3 , and x_2x_3 were insignificant to the responses within variables studied.

3.4. Percentage MG dye removal

With reference to Table 5, IR was found to be the most influential factor on MG dye removal followed by activation temperature as shown by high F -value.

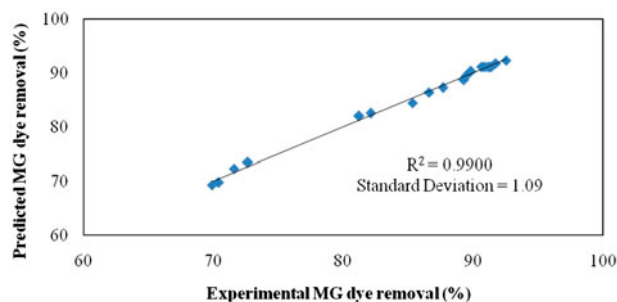


Fig. 1. Predicted vs. experimental MG removal of RSAC.

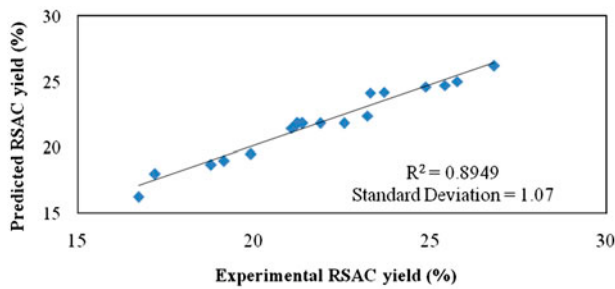


Fig. 2. Predicted vs. experimental RSAC yield.

Fig. 3 illustrates the combined effect of activation temperature (x_1) and IR (x_3), while the activation time (x_2) was kept at zero level (2 h). This plot of activation temperature and IR was chosen due to the interaction of x_1x_3 that gives the highest F -value of 9.61 with Prob. $> F$ is 0.0112, compared to other combination of variables (Table 5). The Prob. $> F$ value less than 0.05 indicate that the combination of two variables selected have strong interaction with each other. MG dye removal increased with increase in activation temperature and IR. From Fig. 3, the maximum MG dye removal was achieved at activation temperature ranging between 750 and 830 °C and IR ranging between 2 and 3.0. Similar observation was obtained by Xin-hui

and co-workers. They found out that the activation temperature and IR play important roles in the preparation of AC from *Jatropha* hull [42]. High activation temperature was needed for pore development and intercalation of potassium metal to the carbon material during activation. However, excessive temperature could reduce the surface area and thus decrease the dye adsorption. The possible reason is that when the surface area of AC prepared reaches the maximum value, further increase in both activation time and temperature resulted in excess activation leading to the collapse of some pore structures; this consequently leads to decrease in surface area. In addition, excessive amount of impregnating agent can demolish the pore structure formed. A similar observation was reported during the preparation of AC by microwave heating and KOH activation [43].

3.5. RSAC yield

The three variables studied gave significant effects on RSAC yield as shown in Table 6. Fig. 4 shows the effect of activation temperature and activation time on the RSAC yield, while IR fixed at zero level (IR = 2.25). Meanwhile, Fig. 5 shows the effect of activation temperature and IR on the same response, with

Table 4
Matrix for RSAC preparation variables and responses

Run	Level	RSAC preparation variables						
		Activation temperature, x_1 (°C)	Activation time, x_2 (h)	IR, x_3	MG removal, Y_1 (%)	RSAC yield, Y_2 (%)		
1	-1	-1	-1	700.00	1.00	1.00	70.42	25.78
2	+1	-1	-1	850.00	1.00	1.00	81.22	23.30
3	-1	+1	-1	700.00	3.00	1.00	72.65	24.88
4	+1	+1	-1	850.00	3.00	1.00	82.12	17.20
5	-1	-1	+1	700.00	1.00	3.50	85.32	23.23
6	+1	-1	+1	850.00	1.00	3.50	92.54	21.21
7	-1	+1	+1	700.00	3.00	3.50	87.68	22.56
8	+1	+1	+1	850.00	3.00	3.50	91.19	16.73
9	-1.682	0	0	648.87	2.00	2.25	71.57	23.69
10	1.682	0	0	901.13	2.00	2.25	89.83	19.15
11	0	-1.682	0	775.00	0.32	2.25	86.61	25.43
12	0	1.682	0	775.00	3.68	2.25	89.27	18.78
13	0	0	-1.682	775.00	2.00	0.15	69.89	26.82
14	0	0	1.682	775.00	2.00	4.35	89.43	19.91
15	0	0	0	775.00	2.00	2.25	91.29	21.38
16	0	0	0	775.00	2.00	2.25	90.96	21.25
17	0	0	0	775.00	2.00	2.25	90.62	21.89
18	0	0	0	775.00	2.00	2.25	91.73	21.37
19	0	0	0	775.00	2.00	2.25	90.82	21.07
20	0	0	0	775.00	2.00	2.25	91.38	21.19

Table 5
ANOVA analysis for MG dye removal for RSAC

Source	Sum of squares	Degree of freedom (DF)	Mean square	F-value	Prob. > F
Model	1,175.16	9	130.57	110.33	<0.0001
x_1	278.84	1	278.84	235.60	<0.0001
x_2	5.43	1	5.43	4.59	0.0578
x_3	506.65	1	506.65	428.09	<0.0001
x_1^2	182.14	1	182.14	153.90	<0.0001
x_2^2	14.28	1	14.28	12.06	0.0060
x_3^2	221.76	1	221.76	187.38	<0.0001
x_1x_2	3.18	1	3.18	2.68	0.1325
x_1x_3	11.38	1	11.38	9.61	0.0112
x_2x_3	0.56	1	0.56	0.47	0.5065

Table 6
ANOVA analysis for RSAC yield

Source	Sum of squares	Degree of freedom (DF)	Mean square	F-value	Prob. > F
Model	125.84	6	20.97	18.45	<0.0001
x_1	48.16	1	48.16	42.37	<0.0001
x_2	39.87	1	39.87	35.08	<0.0001
x_3	26.58	1	26.58	23.38	0.0003
x_1x_2	10.15	1	10.15	8.93	0.0105
x_1x_3	0.67	1	0.67	0.59	0.4573
x_2x_3	0.43	1	0.43	0.38	0.5501

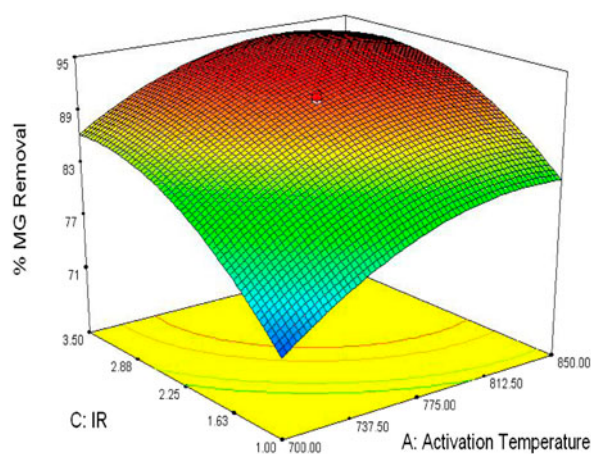


Fig. 3. Response surface plot of MG dye removal of RSAC (effect of activation temperature and IR, activation time = 2 h).

activation time fixed at zero level ($t = 2$ h). RSAC yield was found to decrease with increase in activation temperature, activation time, and IR. The highest RSAC yield was obtained when all variables were at minimum point. The weight loss was due to the process of pyrolysis which promotes pore development and new pore creation. High temperature had caused a reduc-

tion in RSAC yield due to occurrence of elimination and dehydration reactions [44]. This result was in agreement with the work reported in the preparation of waste tea AC for Methylene blue dye removal [45]. It also agreed with the studies carried out on preparation of highly porous carbon from fire wood by KOH etching and CO_2 gasification for the adsorption of dyes and phenols from water [46].

3.6. Optimization of operating parameters

The objective of the experimental design was to find the optimum preparation conditions so that the high AC's yield with high dye removal can be achieved. However, these responses have different interest regions on the factors. As the dye removal increases, the AC yield decreases and vice versa. Hence, two optimum operating conditions must be determined. Table 7 shows the model validation of RSAC for MG dye removal, and AC yield. Optimized parameters were selected based on higher desirability. Optimum condition selected was verified experimentally. Design Expert Software version 7.1.5 (STAT-EASE Inc., Minneapolis, USA) was used to optimize the parameters where the targets were set at maximum values, while the values of variables were set in

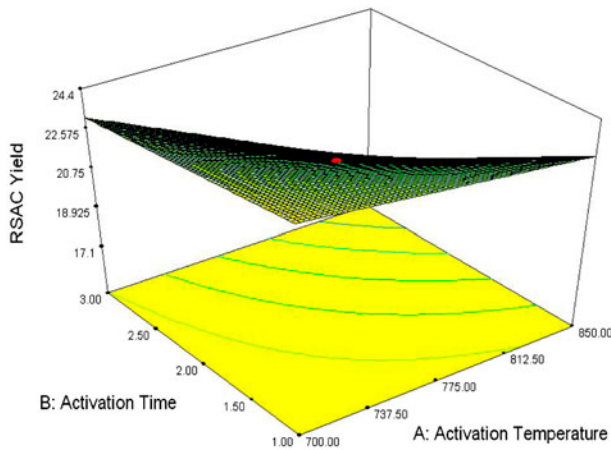


Fig. 4. Response surface plot of RSAC yield (effect of activation temperature and activation time, IR = 2.25).

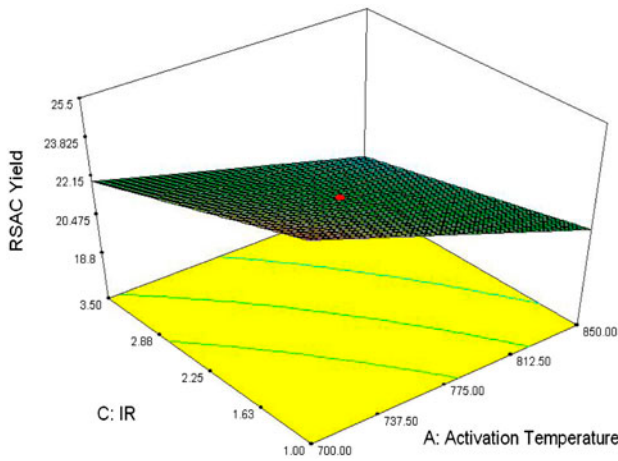


Fig. 5. Response surface plot of RSAC yield (effect of activation temperature and IR, activation time = 2 h).

range being studied. Table 7 shows model validation for MG dye removal by RSAC. The adsorbent was prepared at optimum conditions. The predicted and experimental values for the two responses for the activated carbon prepared are also presented in the same Table. The optimum conditions of MG dye removal by RSAC are; 802 °C, 1.0 h, and 2.4, respectively. The MG dye percent removal obtained is 91.45%. It also resulted in 22.56% RSAC yield.

Model desirability approaching unity and with low error value portray the applicability of model towards the responses. From Table 7, relatively small errors less than 3% between the predicted and the actual value was observed, which indicated that the model is suitable and sufficient to predict the responses. The optimized RSAC prepared was further characterized to determine its physical and chemical characteristics.

Table 7
Model validation for RSAC prepared for MG dye removal

Activated carbon	Model desirability	Activation temperature, x_1 (°C)	Activation time, x_2 (h)	IR, x_3	MG dye removal (%)		AC yield (%)	
					Predicted	Experimental	Predicted	Experimental
RSAC	0.977	802	1.0	2.4	91.45	89.77	23.12	22.56
					1.84	1.84	2.42	2.42

Table 8
Pore characteristics and surface area of the samples

Sample	BET surface area (m ² /g)	Mesopore surface area (m ² /g)	Total pore volume (cm ³ /g)	Average pore diameter (nm)
RS raw	2.08	–	–	–
RS char	75.93	57.82	0.110	5.68
RSAC	865.14	540.07	0.443	5.82

Table 9
FTIR spectrum band for RS, RS char, and RSAC

Assignments	Band positions (cm ⁻¹)		
	RS raw	RS char	RSAC
O–H stretching of hydroxyl group	3,865–3,734	3,876–3,741	3,892
C≡C stretching of alkyne group	2,341	2,426–2,212	2,422
C=O stretching of lactones, ketones, and carboxylic anhydrides	1,735	1,739	
C=C stretching of aromatic ring	1,525	1,523	1,523
C–N stretching of amines	1,242	1,242	
C–O groups stretching in ester, ether or phenol group	987	981	983
–C≡C–H–C–H bend in functional group	713–551	732	740

3.7. Characterization of prepared adsorbent

3.7.1. Pore characteristics and surface area

The pore characteristics of RSAC are given in Table 8. The surface area of the prepared adsorbent increases significantly. RSAC has a relatively high BET surface area of 865.14 m²/g and the total pore volume of 0.443 cm³/g. The high BET surface area and total pore volume were due to the activation process used, which involved both chemical and physical activating agents. It was activated with KOH and subsequently gasified with CO₂. Diffusion of KOH and CO₂ molecules into the adsorbent resulted in KOH-carbon and CO₂-carbon reactions which facilitated the development of more pores on the surface of RSAC. The average pore diameter of RSAC is 5.82 nm. It belongs to the macropore region according to IUPAC classification [47]. The significant increase in surface area was attributed to intercalation of potassium metal from intermediate reaction of KOH with carbon [48].

3.7.2. Surface morphology (SEM)

SEM was used to characterize the surface morphology of the adsorbent as shown in Fig. 6. No pore was detected on RS whereas large pores were clearly seen on the surface of the RSAC. The well-developed pores resulted in larger surface area and more porous structure of the RSAC; this further enhanced the adsorption process [49]. RSAC has heterogeneous pore

Table 10
Proximate analysis of adsorbents prepared

Sample	Proximate analysis (%)			
	Moisture	Volatile	Fixed carbon	Ash
RS	8.80	67.39	19.56	4.25
RS char	3.56	26.45	66.18	3.81
RSAC	2.44	18.23	75.74	3.59

distribution. High activation temperature and KOH used for impregnation were believed to be responsible for the pore development in RSAC. The C-KOH reaction rate was increased during the activation process, which resulted in higher carbon “burn-off” and porosity on the adsorbent. The C-KOH reaction also increased the porosity of the existing pore as well as creating new pores [50]. Besides, the physiochemical treatment was able to produce porous RSAC thus increasing the surface area that will enhance its adsorption capacity.

3.7.3. Surface chemistry

FTIR analysis for RS, RS char, and RSAC are shown in Table 9 and also illustrated in Fig. 7. The spectra revealed that various functional groups are detected on the surface of adsorbent prepared. Table 9 shows presence of O–H stretching of hydroxyl group

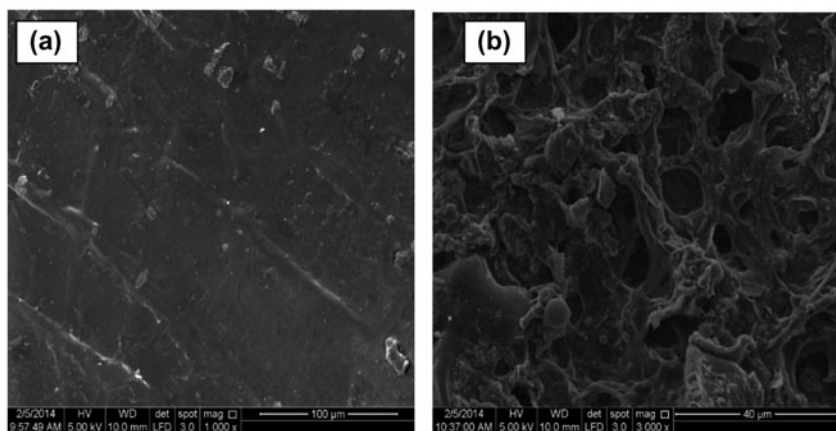


Fig. 6. SEM micrographs of (a) RS (3,000×) and (b) RSAC (3,000×).

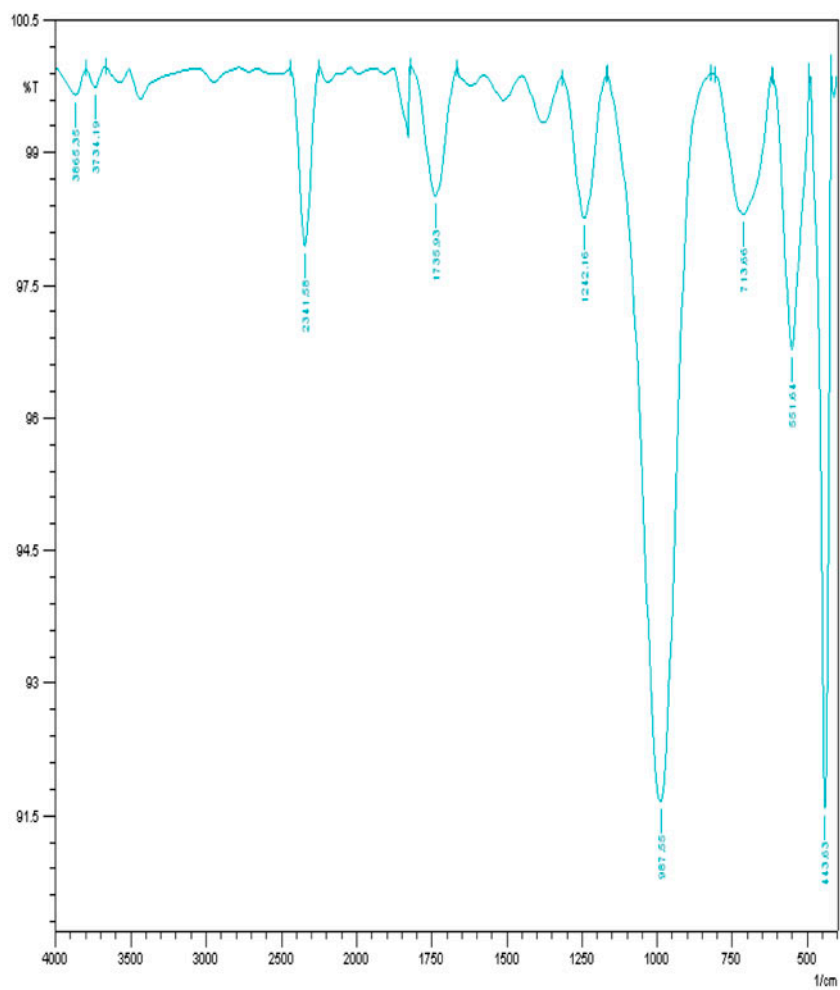


Fig. 7. FTIR spectra of (a) RS, (b) RS char, and (c) RSAC.

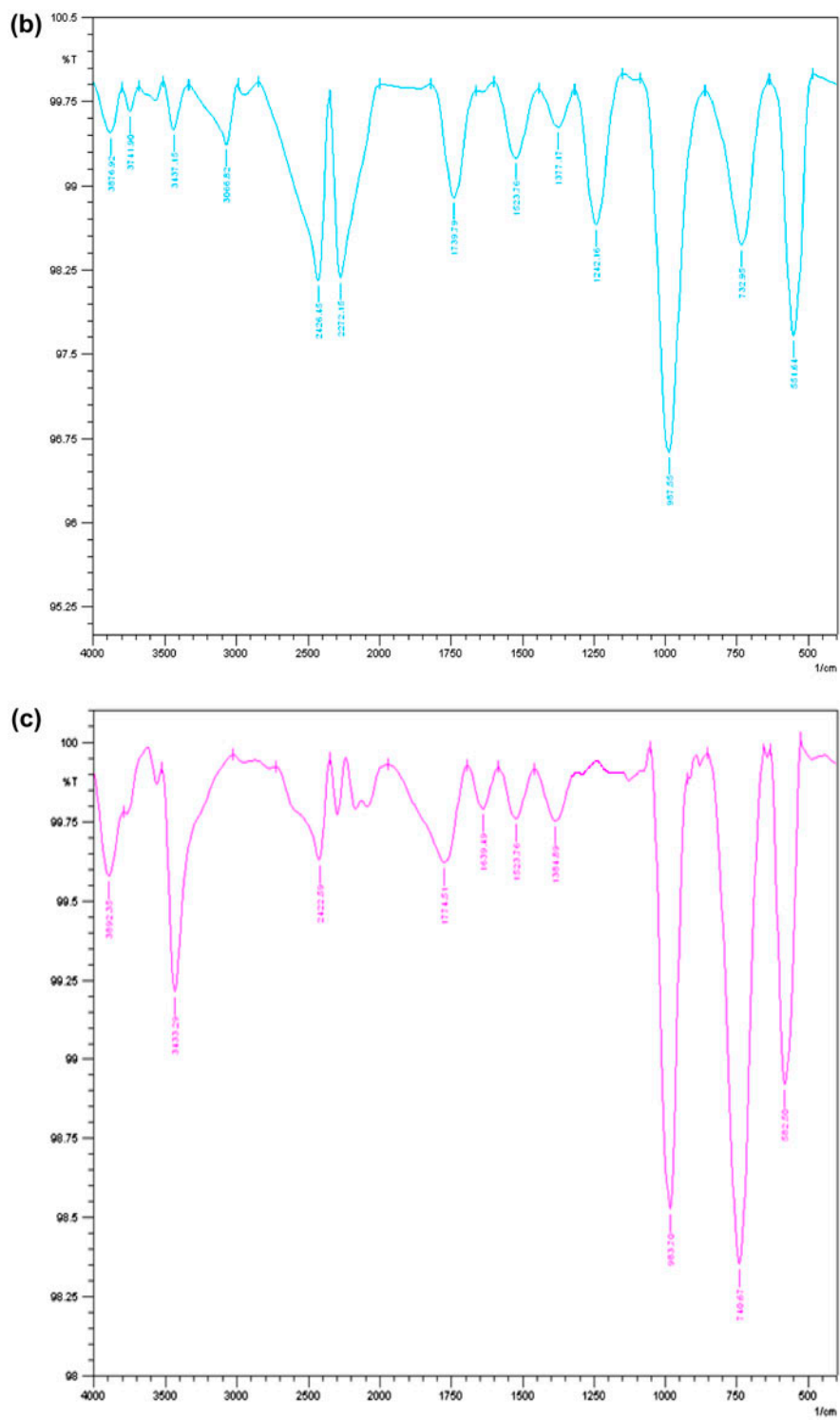


Fig. 7. (Continued).

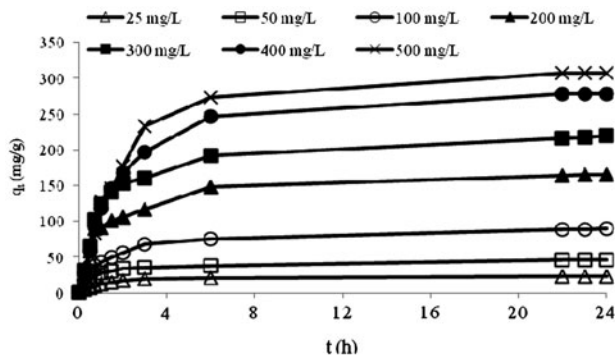


Fig. 8. Plot of MG dye adsorption uptake against adsorption time at various initial concentrations at 30°C.

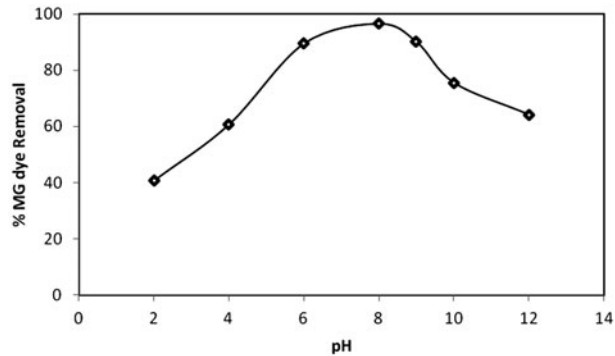


Fig. 9. Effect of pH on percentage MG dye removal.

as major peaks around 3,865–3,734 cm^{-1} , and 3,982 cm^{-1} in RS and RSAC, respectively. The peaks at 1,735 and 1,242 cm^{-1} in RS vanished from RSAC, indicating disappearance of both oxygen and amine group functionalities. In fact, most functional groups reduced after the activation process. Other major peaks detected are $\text{C}\equiv\text{C}$ stretching of alkyne group at 2,422–2,341 cm^{-1} , $\text{C}=\text{C}$ stretching of aromatic ring at 1,525–1,523 cm^{-1} and $\text{C}-\text{O}$ groups stretching in ester, ether or phenol groups at 1,739–1,735 cm^{-1} , respectively. From the FTIR spectra, the surface chemistry of the char and RSAC was different from their precursor as many of the functional groups reduced while others disappeared due to the thermal degradation [51].

3.7.4. Proximate analysis

Table 10 reports the proximate analysis of the raw, char, and activated carbon prepared. RS were found to be rich in moisture and volatile matter. The moisture and volatile matter decreased from precursor to RSAC. The high temperature during carbonization

Table 11
Isotherm parameters for adsorption of MG dye onto RSAC at 30°C

	Langmuir	Freundlich	Temkin	Dubinin–Radushkevich (DR)	Sips	Radke–Prausnitz (RP)	Vieth–Sladek (VS)	Brouers–Sotolongo (BS)
RSAC	$q_m = 341.37$ $k_L = 0.035$ $R_L = 0.054$ $R^2 = 0.982$	$k_F = 23.55$ $n_F = 1.946$ $1/n_F = 0.514$ $R^2 = 0.985$	$B_T = 58.72$ $A_T = 0.687$ $R^2 = 0.963$	$q_s = 16.52$ $E = 5.38$ $b_{DR} = 0.0018$ $R^2 = 0.890$	$q_m = 351.60$ $k_S = 0.028$ $m_S = 1.008$ $R^2 = 0.798$	$q_m = 327.72$ $k_{RP} = 0.037$ $m_{RP} = 1.020$ $R^2 = 0.854$	$k_{VS} = 0.0069$ $q_m = 332.69$ $B_{VS} = 0.033$ $R^2 = 0.857$	$q_m = 321.66$ $k_{BS} = 0.026$ $\alpha = 0.906$ $R^2 = 0.859$

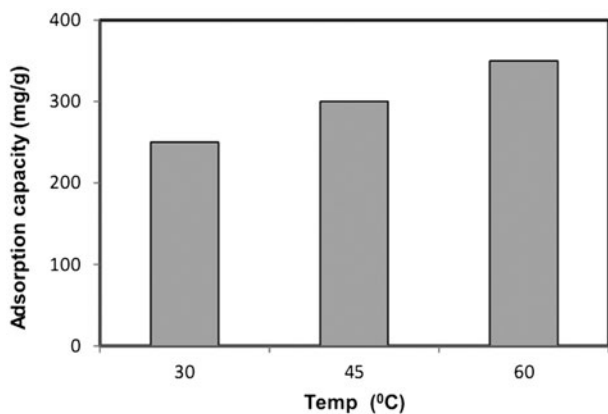


Fig. 10. Effect of solution temperature on MG dye adsorption onto RSAC.

and activation processes caused a reduction in both the volatile matter and moisture content. However, the fixed carbon increased sharply from raw material to RSAC prepared. This was due to the heat supplied during carbonization process which initiates thermal degradation process. The volatile substance becomes unstable at high temperature; their bonds are broken leading to volatilization [52].

3.8. Batch adsorption studies

3.8.1. Effect of initial dye concentration

For effective dye adsorption, the initial dye concentration is an important factor. In Fig. 8, adsorption capacities (mg/g) are plotted against different initial dye concentrations. From the figure, the adsorption capacity of RSAC increased with increase in initial dye concentration up to a certain level, after which the process is almost saturated. The adsorption of MG dye was quite rapid at the initial stage, the equilibrium time for dye adsorption at concentrations (25–200 mg/L) was 6 h. The adsorption was then gradual with increase in contact time. After 22 h of contact, no obvious variation in MG dye adsorbed was noticed for concentrations (400–500 mg/L). The equilibrium time for these concentrations is 22 h. The increase in MG dye uptake capacity can be explained by the fact that increasing concentration gradient of dye provides an increasing driving force to overcome all mass transfer resistance of the dye molecule between the aqueous and solid phase, leading to an increased equilibrium uptake capacity until saturation is achieved. On the contrary, the percentage removal of dye decreases with increase in initial dye concentration. This can be explained by the fact that

all adsorbents have a limited number of active sites and porous channel, which becomes saturated at a certain dye concentration. A similar trend has been reported in the adsorptive removal of malachite green using banana stalk based activated carbon [53].

3.8.2. Effect of solution pH on MG dye adsorption

The pH of solution is an important monitoring parameter in dye adsorption, as it affects the surface charge of the adsorbent material and the degree of ionization of the dye molecule. It is also directly related with competition ability of hydrogen ions with the adsorbate molecules to the active sites on the adsorbent surface. In Fig. 9, the percentage removal of MG dye from aqueous solution is plotted against different pH of solution. From Fig. 9, it is depicted that the percentage of MG dye removed by RSAC increase with the increase in pH of the dye solution, appreciably up to pH 8.0 corresponding to 96.7%. Further increase in pH leads to a reduction in the amount of dye adsorbed. This trend may be explained as follows; at low pH values, protonation of the functional groups present on the adsorbent surface easily takes place. The surface of the adsorbent becomes positively charged, since the dye is positively charged, a decrease in adsorption took place as a result of electrostatic repulsion. However, as the pH of the dye solution increases, a considerable increase in dye binding capacity is observed due to strong electrostatic attraction between negatively charged sites on the adsorbent and the positively charged MG dye cations. Similar trend was observed in the batch removal of crystal violet from aqueous solution by H₂SO₄ modified sugar cane Bagasse and the adsorptive removal of MG dye using coconut shell-based activated carbon [54,55].

3.8.3. Effect of solution temperature

Temperature has a pronounced effect on the adsorption process since a change in temperature promotes changes in the equilibrium capacity of the adsorbent [56]. Therefore, the effect of solution temperature on dye removal was studied by varying the solution temperature from 30 to 60°C. The adsorption capacity, q_t increased with the increased in temperature suggesting that the adsorption was an endothermic process (Fig. 10). Increasing the temperature is known to increase the mobility or the rate of diffusion of the adsorbate molecules across the external boundary layer and in the internal pores of the adsorbent particle. At higher temperatures, chemical interaction between

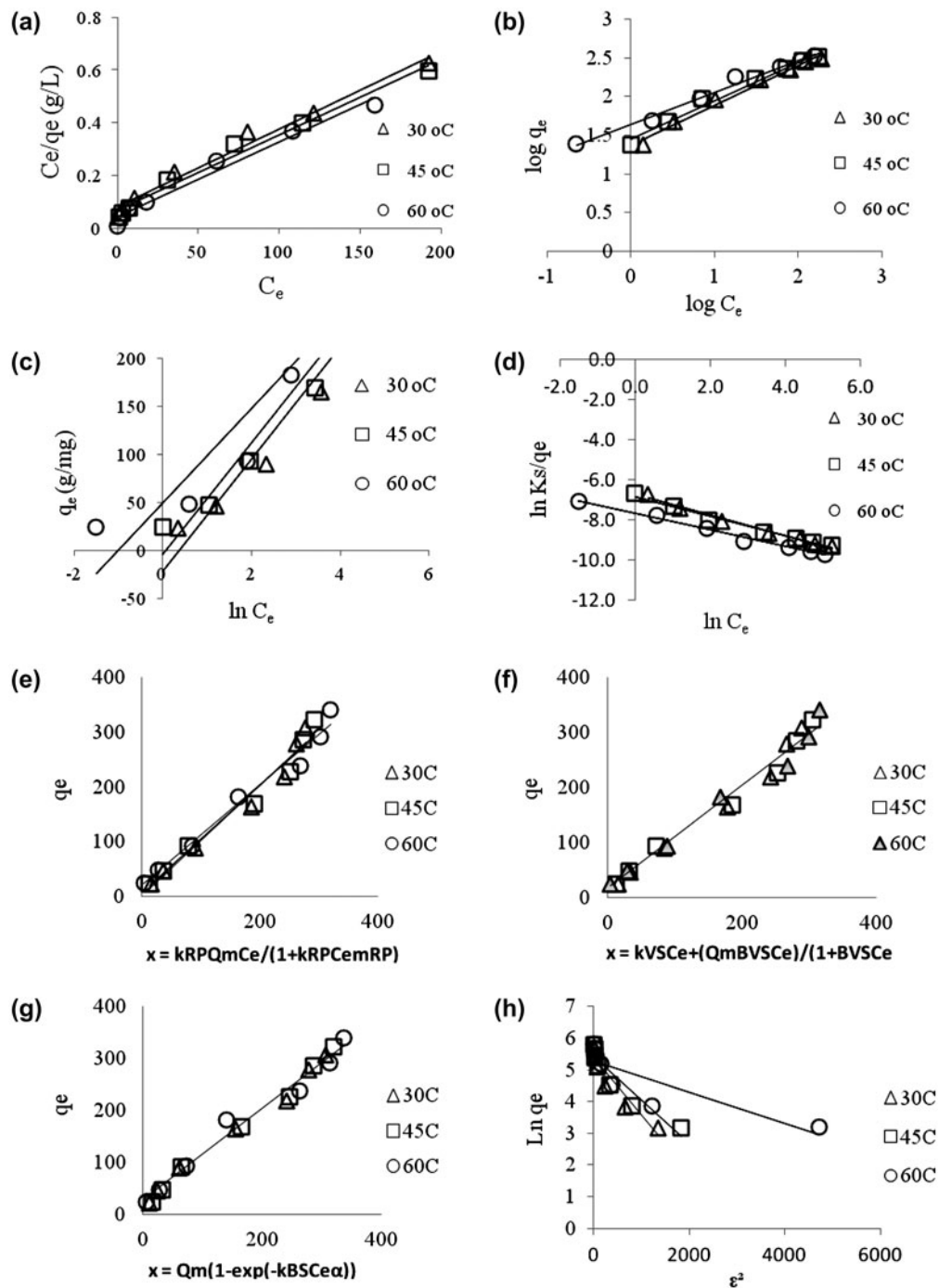


Fig. 11. Plots of (a) Langmuir, (b) Freundlich, (c) Temkin, (d) Sip, (e) Radke–Prausnitz, (f) Vieth–Sladek, (g) Brouers–Sotolongo, and (h) Dubinin Radushkevich isotherms for MG dye adsorption onto RSAC.

adsorbate and adsorbent increases resulting in creating higher affinity between the active sites and the adsorbates [57]. In addition, changing the temperature will alter the equilibrium capacity of the adsorbent for a particular adsorbate. Ahmad and Alrozi also reported a similar trend for the adsorption of reactive dye by

mangosteen peel [44]. This may be a result of increase in the mobility of the dye with increasing temperature whereby an increase in number of molecules will also acquire sufficient energy to undergo an interaction with active sites at the surface [58]. Besides, chemical interaction between the adsorbate and surface

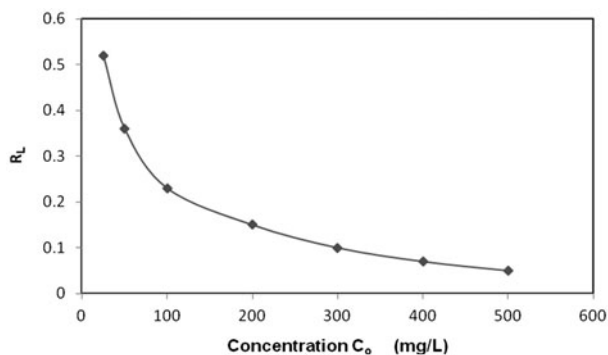


Fig. 12. Plots of separation factor, R_L vs. MG dye initial concentration for adsorption of MG dye onto RSAC at 30°C.

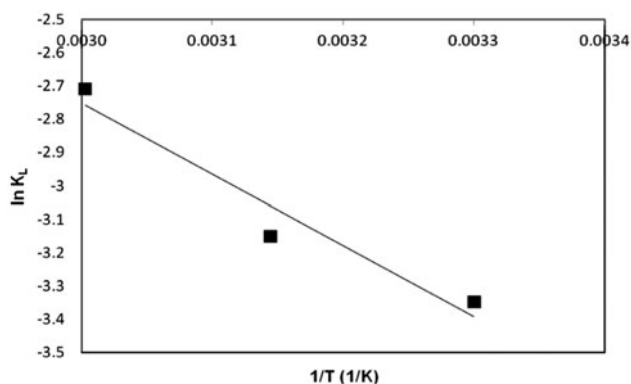


Fig. 13. Plots of $\ln k_L$ vs. $1/T$ for adsorption of MG dye onto RSAC.

functionalities of adsorbent might also contributed to the increase in adsorption capacity.

3.9. Adsorption isotherm

The adsorption isotherm signifies the amount of molecules distributed between the liquid phase and the solid phase when the adsorption process reaches equilibrium state. In this study, the adsorption isotherms studied were Langmuir, Freundlich, Temkin, Sips, Radke–Prausnitz (RP), Vieth–Sladek (VS), Brouers–Sotolongo (BS), and Dubinin–Radushkevich (DR) isotherm models. The linearized forms of all these equations were applied to fit the equilibrium data. The R^2 values from each isotherm model were compared to fit the adsorption data whereby the closer the R^2 to unity, the better the fit. Fig. 11 shows the plot of the linearized isotherm equations for MG dye removal at temperature 30, 45, and 60°C for RSAC.

Table 11 summarizes the constants obtained for the adsorption of MG dye onto RSAC at 30°C.

Based on the R^2 values in Table 11, the adsorption isotherm fitted the data in the order of Freundlich > Langmuir > Temkin > D–R > B–S > V–S > R–P > Sips for RSAC. For adsorption of MG dye at the three temperatures studied, Freundlich isotherm fitted most ($R^2 > 0.985$) with the data which indicates that a multilayer sorption took place at heterogeneous surface of the adsorbent. The Freundlich isotherm model applies to adsorption on heterogeneous surfaces with interaction between adsorbed molecules. From the table, the n_F value for RSAC was greater than 1, indicating that the adsorption is favorable [59]. k_F is one of the Freundlich constants which measure the adsorption capacity of the adsorbent. From Table 11, the high k_F value obtained represents the amount of dye adsorbed onto RSAC per unit equilibrium concentration. k_F value was calculated as 23.55 mg/g $(L/mg)^{1/n}$. The monolayer adsorption capacity, q_m is 341.37 mg/g. The Dubinin–Radushkevich (D–R) isotherm model was used to characterize the porosity and the apparent adsorption free energy. If the free energy, E obtained ranged between 8 and 16 kJ/mol, it is a chemisorption adsorption process; if the E value is below 8 kJ/mol, it is a physisorption adsorption process [31]. From Table 11, E value is 5.38 kJ/mol representing physisorption process.

The essential characteristics of Langmuir equation can be expressed in terms of dimensionless separation factor, R_L where the parameter R_L implies the nature of the adsorption process. Fig. 12 shows the plot of the R_L vs. the MG initial dye concentration for adsorption of MG dye onto RSAC at 30°C. Similar plots were obtained for adsorption systems at 45 and 60°C (Fig. 13). From the figure, R_L values obtained for the adsorption of MG dye ranged between 0 and 1, showing that the adsorption is favorable. Increasing the concentration from 25 to 500 mg/L demonstrated a gradually decrease of R_L , indicating that sorption process was also favorable at high initial dye concentration.

3.10. Batch kinetic studies

Four kinetic models were applied to study the kinetics of the adsorption process and also to determine the diffusion mechanism of the adsorption system. They are: pseudo-first-order, pseudo-second-order, Elovich and Avrami models. Fig. 14(a)–(d) shows the linearized plots of pseudo-first-order kinetic, pseudo-second-order kinetic, Elovich, and Avrami model for MG dye adsorption onto RSAC at

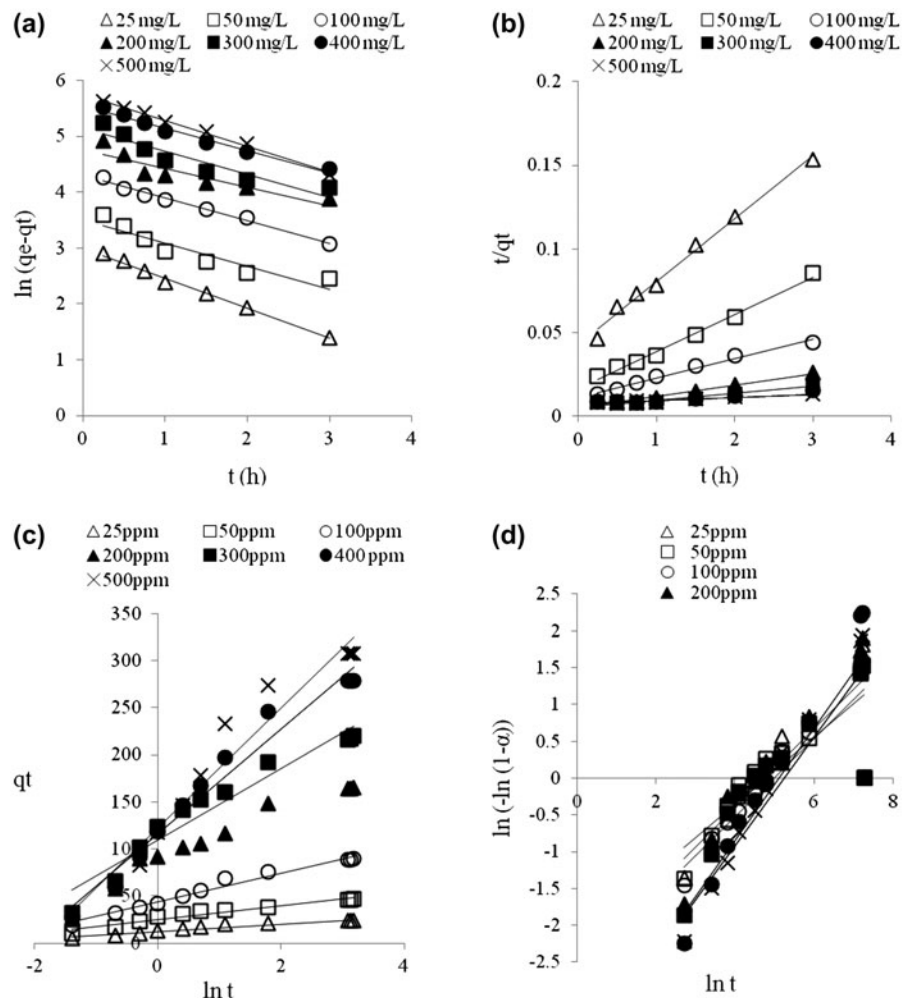


Fig. 14. Linearized plots of (a) pseudo-first-order, (b) pseudo-second-order, (c) Elovich, and (d) Avrami kinetic model for MG dye adsorption onto RSAC at 30°C.

30°C for various initial dye concentration. Similar plots are obtained for the adsorption process at 45 and 60°C (Fig. 13).

Pseudo-second-order kinetic model fits the data most when compared to other models. In fact, as can be seen from the figure, the experimental data for adsorption of MG dye were not correlated well by the pseudo-first-order kinetic model compared to the pseudo-second-order kinetic model. All the experimental and calculated q_e values, together with the constants, R^2 and Δq_t values obtained from the pseudo-first-order, pseudo-second-order, Elovich and Avrami model for adsorption onto RSAC at 30°C, are reported in Table 12. From Table 12, it can be seen that most of the R^2 values obtained from the pseudo-second-order model were close to unity and the highest among all models, showing that the adsorption of MG dye onto RSAC fitted most to this model at all

initial concentrations. Besides, pseudo-second-order was found to have lowest Δq_t compared to other models. The R^2 values obtained for the pseudo-first-order model did not show a consistent trend which resulted in quite large Δq_t . This result indicates that the adsorption of MG dye onto RSAC does not follow the pseudo-first-order model.

In fact, there was a consistent trend in the k_2 values obtained for MG dye adsorption, the rate constant was found to decrease as the initial dye concentration increased which indicate that dye with lower initial concentration reached equilibrium faster than higher concentration. The reason for this behavior can be attributed to the lower competition for the adsorbent surface sites at lower concentration. At higher concentrations, the competition for the surface active sites will be high and consequently lower adsorption rates obtained [60]. Meanwhile, Elovich and Avrami kinetic

Table 12
Kinetic model constant parameters for adsorption of MG dye onto RSAC at 30°C

Model	Kinetic parameters	Initial MG dye concentration (mg/L)						
		25	50	100	200	300	400	500
Pseudo-first-order	$Q_{e,exp}$ (mg/g)	23.58	46.66	89.77	164.83	219.60	278.70	307.76
	k_1 (min^{-1})	0.541	0.417	0.404	0.335	0.414	0.404	0.466
	$Q_{e,cal}$ (mg/g)	20.14	33.43	73.43	116.99	170.78	258.08	314.16
	R^2	0.994	0.877	0.987	0.811	0.862	0.977	0.994
	Δq_t (%)	14.58	28.34	18.22	29.02	22.23	7.39	2.07
Pseudo-second-order	k_2 (min^{-1})	0.033	0.030	0.011	0.008	0.003	0.001	0.001
	$Q_{e,cal}$ (mg/g)	26.49	45.02	86.78	150.17	238.35	391.71	529.49
	R^2	0.997	0.991	0.993	0.961	0.929	0.980	0.998
	Δq_t (%)	2.32	3.50	3.33	8.89	8.53	4.54	2.04
Elovich	α (mg/g/min)	5.504	4.284	1.0783	0.770	0.469	0.141	0.106
	β (g/mg)	3.975	7.277	15.433	27.597	37.971	55.953	63.830
	R^2	0.941	0.950	0.981	0.952	0.910	0.970	0.958
	Δq_t (%)	2.60	5.47	17.65	10.37	11.26	6.16	5.14
Avrami	k_{AV} (min^{-1})	0.0085	0.008	0.0067	0.0080	0.0067	0.0059	0.0194
	n_{AV}	0.534	0.453	0.515	0.553	0.529	0.761	0.733
	R^2	0.743	0.731	0.782	0.736	0.746	0.797	0.818

models seem to be insufficient to describe MG dye adsorption due to the low R^2 values obtained. This indicates that there are more than one mechanism involved in the adsorption process. Pseudo-second-order kinetic model fitted the adsorption data most due to high values of R^2 (closer to unity) and low Δq_t values (indicating good agreement between calculated and experimental q_e values). Similar results were obtained by other researchers using different adsorbents; bamboo-based AC [27,61] and mangosteen peel [44].

3.11. Adsorption thermodynamic studies

Fig. 15 shows the plot of $\ln k_L$ vs. $1/T$ for adsorption of MG dye onto RSAC at temperatures 30, 45 and 60°C respectively. Meanwhile, Fig. 16 illustrates the plot of $\ln k_2$ vs. $1/T$ for adsorption of MG dye onto RSAC. From these plots, the minimum energy that reactants must have for the reaction to proceed, E_a value was obtained. The figure gave linear lines having negative slopes thus giving positive activation energy value. Table 13 shows calculated values of ΔH° , ΔS° , and ΔG° for the adsorption process at different temperatures. From Table 13, it can be seen that the results are consistent with the results obtained earlier on the effects of solution temperature on the adsorption process where the adsorption capacity increased with increase in temperature from 30 to 60°C. From Table 13, the ΔH° value obtained is less 80 kJ/mol, suggesting that the adsorption process follows physisorption mechanism. Similarly, the positive value of ΔH° indicates the endothermic nature of the process. Diffusion rate of adsorbate molecules across the external boundary layers and internal pores of adsorbent increased as temperature increases confirming an endothermic adsorption process [59]. Generally E_a for chemisorption is in the range of 80–400 kJ/mol, while for physisorption it is 1–40 kJ/mol. The E_a value is less than 40 kJ/mol indicating that the adsorption of MG dye onto RSAC follows physisorption mechanism

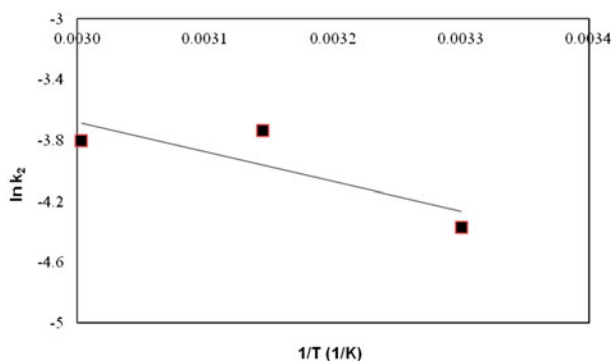


Fig. 15. Plots of $\ln k_2$ vs. $1/T$ for adsorption of MG dye onto RSAC.

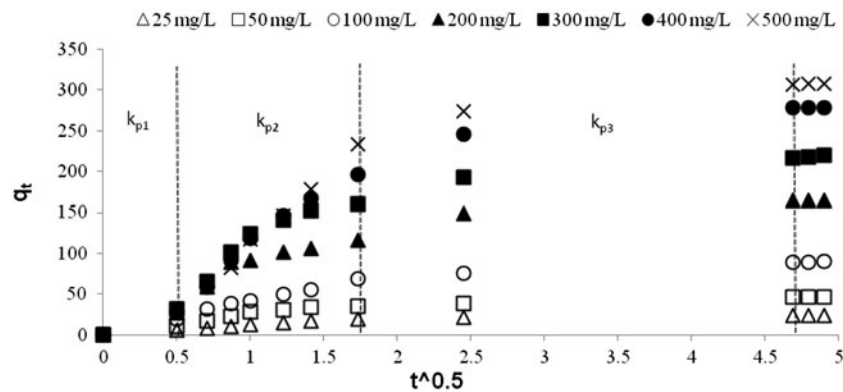


Fig. 16. Plots of intraparticle diffusion model for MG dye adsorption onto RSAC at 30°C.

Table 13
Thermodynamic parameters for adsorption of MG dye onto RSAC

Activated carbon	ΔH° (kJ/mol)	ΔS° (kJ/mol)	E_a (kJ/mol)	$-\Delta G^\circ$ (kJ/mol)		
				303 K	318 K	333 K
RSAC	17.78	30.46	16.07	8.44	8.33	7.50

[62]. In this study, the ΔS° value obtained for MG adsorption is positive. This is the normal consequence of the physical adsorption phenomenon, which takes place through electrostatic interactions. ΔG° values obtained for the adsorption process are negative and low (<20 kJ/mol). Low ΔG° value connotes a physisorption mechanism [57].

3.12. Adsorption mechanism

Fig. 16 shows the intraparticle diffusion plot for the adsorption of MG dye onto RSAC at 30°C for various initial dye concentrations. Similar trends were observed for the adsorption process at 45 and 60°C (Fig. 13). From the figure, the plot has three different regions; (i) a sharper region completed within the first 30 min (0.5 h) was the instantaneous adsorption where the mass transfer of dye molecules from the bulk solution to the adsorbent surface occurred [63], (ii) gradual adsorption stage, where the intraparticle diffusion was the rate limiting step, (iii) the final equilibrium stage where intraparticle diffusion started to slow down due to the extremely low adsorbate concentration in the bulk solution [51]. The values of the intraparticle diffusion model constants (k_p and C) obtained for the three regions from the plot of q_t vs. $t^{1/2}$ are presented in Table 14. As can be seen from the table, the k_p values (k_{p1} and k_{p2}) for the three regions increased as the

initial concentration increases. Increase in the initial dye concentration owing to the increase in the driving force (concentration gradient) results in increasing dye diffusion rate [64]. In addition, constant C was found to increase with increase in initial concentration which indicated that the internal mass transfer was due to the increase in boundary layer thickness. From Fig. 16, the linear lines of the second and third stages did not pass through the origin. It means that intraparticle diffusion was not the only rate limiting mechanism in the adsorption process.

The kinetic data were further analyzed using the Boyd model [65] to distinguish between film diffusion and particle internal diffusion of adsorbate molecules in order to identify the slowest step in the adsorption process [66]. If the plot of B_T vs. time t is a straight line passing through the origin, then the adsorption rate is governed by particle diffusion mechanism, otherwise it is governed by film diffusion mechanism. Fig. 17 illustrates the Boyd plot (B_T vs. t) for adsorption of MG dye onto RSAC at 30°C. According to Senthilkumar, the slowest step in the adsorption process was the internal diffusion if the plot was linear and passes through the origin [66]. As can be seen from the figure, the linear lines at all initial concentrations did not pass through the origin, indicating that the adsorption process is mainly governed by external mass transfer or film-diffusion-controlled mechanism.

Table 14
Intraparticle diffusion model constant and correlation coefficient for adsorption of MG dye onto RSAC at 30°C

MG Initial concentration (mg/L)	k_{p1} (mg/g h ^{1/2})	k_{p2} (mg/g h ^{1/2})	k_{p3} (mg/g h ^{1/2})	C_1	C_2	C_3	$(R_1)^2$	$(R_2)^2$	$(R_3)^2$
25	10.73	7.62	0.41	0	4.45	21.54	1	0.882	0.985
50	20.78	11.02	3.24	0	14.68	30.73	1	0.789	0.939
100	37.34	26.12	3.80	0	16.51	71.06	1	0.946	0.839
200	54.70	44.24	2.71	0	42.23	151.57	1	0.919	0.979
300	63.34	64.23	17.10	0	47.75	135.68	1	0.857	0.981
400	56.87	103.98	0.15	0	6.84	277.93	1	0.950	0.948
500	63.92	126.38	2.34	0	13.48	296.25	1	0.949	0.981

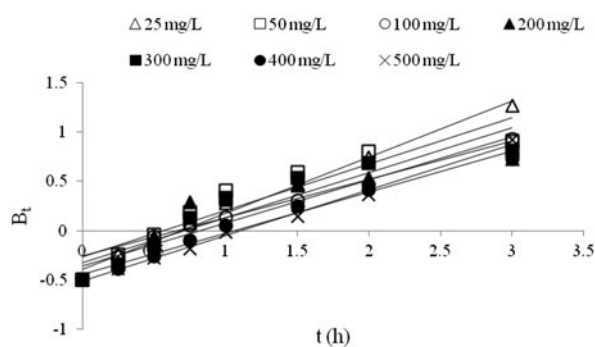


Fig. 17. Boyd plots for adsorption of MG dye onto RSAC at 30°C.

This was due to the differences in the rate of mass transfer in the first and second stages by external mass transfer (film diffusion) where the particle diffusion was the rate limiting step. The first stage of adsorption is attributed to the diffusion in the macropore and the second stage to micropore diffusion.

4. Conclusion

The results obtained in this study clearly showed the potential of RSAC as an effective adsorbent for the removal of MG dye from aqueous solutions. RSM was successfully applied to determine the optimum conditions for maximum percentage MG dye removal and RSAC yield. The optimum conditions of MG removal by RSAC are; 802°C, 1.0 h and 2.4, respectively. The MG dye percent removal obtained is 91.45%. It also resulted in 22.56% RSAC yield. The model employed provided good quality of prediction for the above variables in terms of effective dye removal and a good correlation coefficient, $R^2 = 0.977$ was obtained.

RSAC was successfully prepared and used as adsorbent for the removal of MG dye from an aqueous solution. RSAC has a relatively high BET surface area of 865.14 m²/g and a total pore volume of 0.443 cm³/g comparable to expensive commercially activated carbon. The maximum uptake of MG dye occurred at pH 8.0. The adsorption of dye was highly dependent on the initial dye concentration, contact time, and pH of solution.

Acknowledgments

The financial support in form of grants from USM, the three months USM-TWAS Visiting Researcher Fellowship, FR number: 3240268492 awarded to the corresponding author and the accumulated leave granted to Dr O.S Bello by his home institution to utilize the fellowship is thankfully recognized.

References

- [1] M. Arulkumar, P. Sathishkumar, T. Palvannan, Optimization of Orange G dye adsorption by activated carbon of *Thespesia populnea* pods using response surface methodology, *J. Hazard. Mater.* 186 (2011) 827–834.
- [2] F.C. Wu, R.L. Tseng, High adsorption capacity NaOH activated carbon for dye removal from aqueous solution, *J. Hazard. Mater.* 152 (2008) 1256–1267.
- [3] R.D. Kanamadi, N. Ahalya, T.V. Ramachandra, Low cost biosorbents for dye removal, CES Technical Report 113, 2006.
- [4] T. Min-Yu, L. Su-Hsia, Removal of methyl orange dye from water unto raw and activated montmorillonite in fixed beds, *Desalination* 201 (2006) 71–81.
- [5] P.K. Malik, Use of activated carbons prepared from sawdust and rice-husk for adsorption of acid dyes: a case study of Acid Yellow 36, *Dyes Pigm.* 56 (2003) 239–249.
- [6] J.K. Nafeesa, Adsorption study for trifluralin on Iraqi α -alumina, *J. Baghdad Sci.* 9 (2012) 153–159.
- [7] P. Brown, I.A. Jefcoat, D. Parrish, S. Gill, E. Graham, Evaluation of the adsorptive capacity of peanut hull pellets for heavy metals in solution, *Adv. Environ. Res.* 4 (2000) 19–29.
- [8] K.K. Singh, M. Talat, S.H. Hasan, Removal of lead from aqueous solutions by agricultural waste maize bran, *Bioresour. Technol.* 97 (2006) 2124–2130.
- [9] V.C. Taty-Costodes, H. Fauduet, C. Porte, A. Delacroix, Removal of Cd(II) and Pb(II) ions, from aqueous solutions, by adsorption onto sawdust of *Pinus sylvestris*, *J. Hazard. Mater.* 105 (2003) 121–142.
- [10] Z. Reddad, C. Gerente, Y. Andres P.L. Cloirec, Adsorption of several metal ions onto a low-cost biosorbent: Kinetic and equilibrium studies, *Environ. Sci. Technol.* 36 (2002) 2067–2073.
- [11] K.K. Vasanth, Optimum sorption isotherm by linear and non-linear methods for malachite green onto lemon peel, *Dyes Pigm.* 74 (2007) 595–597.
- [12] R.M. Gong, X.P. Zhang, H.J. Liu, Y.Z. Sun, B.R. Liu, Uptake of cationic dyes from aqueous solution by biosorption onto granular kohlrabi peel, *Bioresour. Technol.* 98 (2007) 1319–1323.
- [13] M.A. Husseini, A. Amer, A. El-Maghraby, A.J. Nahla, Utilization of barley straw as a source of activated carbon for removal of methylene blue from aqueous solution, *Appl. Sci. Res.* 3 (2007) 1352–1358.
- [14] P. Nuttawan, N. Nuttakan, J. Kasetsart, Adsorption of Reactive Dye by eggshell and its membrane, *Nat. Sci.* 40 (2006) 192–197.
- [15] W.T. Tsai, H.R. Chen, K.C. Kuo, C.Y. Lai, T.C. Su, Y.M. Chang, J.M. Yang, The adsorption of methylene blue from aqueous solution using waste aqua cultural shell powders, *J. Environ. Eng. Manage.* 19 (2009) 165–172.
- [16] H.H. Zollinger, *Colour Chemistry-Synthesis, Properties and Application of Organic Dyes and Pigments*, VCH Publishers, New York, NY, 1987.
- [17] Q. Muqing, C. Qian, J. Xu, J. Wu, G. Wang, Studies on the adsorption of dyes into Clinoptilolite, *Desalination* 243 (2009) 286–292.
- [18] G.E. Lorenc, G. Graz, Adsorption characteristics of Congo Red on coal-based mesoporous activated carbon, *Dyes Pigm.* 74 (2007) 34–40.
- [19] R. Mas, H. Mas, S. Kathiresan, The removal of methyl red from aqueous solutions using banana pseudo stem fibers, *Am. J. Appl. Sci.* 6 (2009) 1690–1700.
- [20] L. Lian, L. Guan, L.A. Wang, Use of CaCl₂ modified bentonite for removal of Congo red dye from aqueous solutions, *Desalination* 249 (2009) 797–801.
- [21] P. Belter, E.L. Cussler, W.S. Hu, *Bioseparation: Downstream Processing for Biotechnology*, John Wiley and Sons, New York, NY, 1988, pp. 145–279.
- [22] S. Srivastava, R. Sinha, D. Roy, Toxicological effects of malachite green, *Aquat. Toxicol.* 66 (2004) 319–329.
- [23] E. Bulut, M. Özacar, İ.A. Şengil, Adsorption of malachite green onto bentonite: Equilibrium and kinetic studies and process design, *Microporous Mesoporous Mater.* 115 (2008) 234–246.
- [24] M.M. Wall, Ascorbic acid and mineral composition of longan (*Dimocarpus longan*), lychee (*Litchi chinensis*) and rambutan (*Nephelium lappaceum*) cultivars grown in Hawaii, *J. Food Compos. Anal.* 19 (2006) 655–663.
- [25] M.A. Ahmad, R. Alrozi, Optimization of rambutan peel based activated carbon preparation conditions for Remazol Brilliant Blue R removal, *Chem. Eng. J.* 168 (2011) 280–285.
- [26] N.F. Zainudin, K.T. Lee, A.H. Kamaruddin, S. Bhatia, A.R. Mohamed, Study of adsorbent prepared from oil palm ash (OPA) for flue gas desulfurization, *Sep. Purif. Technol.* 45 (2005) 50–60.
- [27] A.A. Ahmad, B.H. Hameed, Effect of preparation conditions of activated carbon from bamboo waste for real textile wastewater, *J. Hazard. Mater.* 173 (2010) 487–493.
- [28] I. Langmuir, The adsorption of gases on plane surfaces of glass, mica and platinum, *J. Am. Chem. Soc.* 40 (1918) 1361–1403.
- [29] H.M.F. Freundlich, Over the adsorption in solution, *J. Phys. Chem.* 57 (1906) 385–471.
- [30] M.I. Temkin, V. Pyzhev, V. Kinetics of ammonia synthesis on promoted iron catalyst, *Acta Physiochim. USSR* 12 (1940) 327–356.
- [31] M.M. Dubinin, L.V. Radushkevich, Equation of the characteristic curve of activated charcoal, *Proc. Acad. Sci.: Phys. Chem. Sect. USSR* 55 (1947) 331–333.
- [32] R. Sips, On the structure of a catalyst surface, *J. Chem. Phys.* 16 (1948) 490–495.
- [33] W.R. Vieth, K.J. Sladek, A model for diffusion in a glassy polymer, *J. Colloid Sci.* 20 (1965) 1014–1033.
- [34] F. Brouers, O. Sotolongo, F. Marquez, J.P. Pirard, Microporous and heterogeneous surface adsorption isotherms arising from Levy distributions, *Physica A* 349 (2005) 271–282.
- [35] C.J. Radke, J.M. Prausnitz, Adsorption of organic solutes from dilute aqueous solution of activated carbon, *Ind. Eng. Chem. Fundam.* 11 (1972) 445–451.
- [36] S. Lagergren, Zur Theorie der sogenannten Adsorption Geloester Stoffe (On the theory of so-called adsorption of dissolved substances), *Veternskapskad Handlingar.* 24 (1898) 1–39.
- [37] Y.S. Ho, G. McKay, Pseudo-second order model for sorption processes, *Process Biochem.* 34 (1999) 451–465.
- [38] C. Aharoni, M. Ungarish, Kinetics of activated chemisorptions. Part I: The non-Elovichian part of the isotherm, *J. Chem. Soc. Farad. Trans.* 72 (1976) 265–268.

- [39] M. Avrami, Kinetics of phase change. II transformation-time relations for random distribution of nuclei, *J. Chem. Phys.* 8 (1940) 212–224.
- [40] W.J. Weber, J.C. Morris, Kinetics of adsorption on carbon from solution, *J. Sanitary Eng. Div. ASCE* 89 (1962) 31–59.
- [41] F.C. Wu, R.I. Tseng, R.S. Jung, Kinetic modeling of liquid-phase adsorption of reactive dyes and metal ions on chitosan, *Water Res.* 35 (2001) 613–618.
- [42] D. Xin-hui, C. Srinivasakannan, P. Jin-hui, Z. Li-bo, Z. Zheng-yong, Preparation of activated carbon from *Jatropha* hull with microwave heating: Optimization using response surface methodology, *Fuel Process. Technol.* 92 (2011) 394–400.
- [43] Y.B. Ji, T.H. Li, L. Zhu, X.X. Wang, Q.L. Lin, Preparation of activated carbons by microwave heating and KOH activation, *Appl. Surf. Sci.* 254 (2007) 506–512.
- [44] M.A. Ahmad, R. Alrozi, Optimization of preparation conditions for mangosteen peel-based activated carbons for the removal of Remazol Brilliant Blue R using response surface methodology, *Chem. Eng. J.* 165 (2010) 883–890.
- [45] M. Auta, B.H. Hameed, Optimized waste tea activated carbon for adsorption of Methylene Blue and Acid Blue 29 dyes using response surface methodology, *Chem. Eng. J.* 175 (2011) 233–243.
- [46] F.C. Wu, R.L. Tseng, Preparation of highly porous carbon from fir wood by KOH etching and CO₂ gasification for adsorption of dyes and phenols from water, *J. Colloid Interface Sci.* 294 (2006) 21–30.
- [47] IUPAC, IUPAC manual of symbols and terminology, *Pure Appl. Chem.* 31 (1972) 579–638.
- [48] Y. Sudaryanto, S.B. Hartono, W. Irawaty, H. Hindarso, S. Ismadji, High surface area activated carbon prepared from cassava peel by chemical activation, *Bioresour. Technol.* 97 (2006) 734–739.
- [49] O.S. Bello, M.A. Ahmad, Response surface modeling and optimization of remazol brilliant blue reactive dye removal using periwinkle shell-based activated carbon, *Sep. Sci. Technol.* 46 (2011) 2367–2379.
- [50] M. Auta, B.H. Hameed, Preparation of waste tea activated carbon using potassium acetate as an activating agent for adsorption of Acid Blue 25 dye, *Chem. Eng. J.* 171 (2011) 502–509.
- [51] I.A.W. Tan, A.L. Ahmad, B.H. Hameed, Adsorption of basic dye on high-surface-area activated carbon prepared from coconut husk: Equilibrium, kinetic and thermodynamic studies, *J. Hazard. Mater.* 154 (2008) 337–346.
- [52] O.S. Bello, T.A. Fatona, F.S. Falaye, O.M. Osulale, V.O. Njoku, Adsorption of eosin Dye from aqueous solution using groundnut hull-based activated carbon: Kinetic, equilibrium, and thermodynamic studies, *Environ. Eng. Sci.* 29 (2012) 186–194.
- [53] O.S. Bello, M.A. Ahmad, N. Ahmad, Adsorptive features of banana (*Musa paradisiaca*) stalk-based activated carbon for malachite green dye removal, *Chem. Ecol.* 28 (2012) 153–167.
- [54] S. Chakraborty, S. Chowdhury, P. Saha, Batch removal of crystal violet from aqueous solution by H₂SO₄ modified sugarcane bagasse: Equilibrium, kinetic, and thermodynamic profile, *Sep. Sci. Technol.* 47 (2012) 1898–1905.
- [55] O.S. Bello, M.A. Ahmad, Coconut (*Cocos nucifera*) shell based activated carbon for the removal of malachite green dye from aqueous solutions, *Sep. Sci. Technol.* 47 (2012) 903–912.
- [56] Z. Al-Qodah, Adsorption of dyes using shale oil ash, *Water Res.* 34 (2000) 4295–4303.
- [57] O.S. Bello, T.S. Siang, M.A. Ahmad, Adsorption of Remazol Brilliant Violet-5R reactive dye from aqueous solution by cocoa pod husk-based activated carbon: Kinetic, equilibrium and thermodynamic studies, *Asia-Pac. J. Chem. Eng.* 7 (2012) 378–388.
- [58] B.H. Hameed, A.A. Ahmad, Batch adsorption of methylene blue from aqueous solution by garlic peel, an agricultural waste biomass, *J. Hazard. Mater.* 164 (2009) 870–875.
- [59] Y.L. Wang, H.W. Zhou, F.L. Yu, B.Y. Shi, H.X. Tang, Fractal adsorption characteristics of complex molecules on particles—A case study of dyes onto granular activated carbon (GAC), *Colloids Surf., A* 299 (2007) 224–231.
- [60] P. Senthil Kumar, S. Ramalingam, C. Senthamarai, M. Niranjanaa, P. Vijayalakshmi, S. Sivanesan, Adsorption of dye from aqueous solution by cashew nut shell: Studies on equilibrium isotherm, kinetics and thermodynamics of interactions, *Desalination* 261 (2010) 52–60.
- [61] B.H. Hameed, Removal of basic dye from aqueous medium using a novel agricultural waste material: Pumpkin seed hull, *J. Hazard. Mater.* 155 (2008) 601–609.
- [62] M.A. Malana, S. Ijaz, M.N. Ashiq, Removal of various dyes from aqueous media onto polymeric gels by adsorption process: Their kinetics and thermodynamics, *Desalination* 263 (2010) 249–257.
- [63] B.H. Hameed, A.A. Ahmad, N. Aziz, Isotherms, kinetics and thermodynamics of acid dye adsorption on activated palm ash, *Chem. Eng. J.* 133 (2007) 195–203.
- [64] K. Nuithitikul, S. Srikhun, S. Hirunpraditkoon, Kinetics and equilibrium adsorption of Basic Green 4 dye on activated carbon derived from durian peel: Effects of pyrolysis and post-treatment conditions, *J. Taiwan Inst. Chem. Eng.* 41 (2010) 591–598.
- [65] G.E. Boyd, A.W. Adamson, L.S. Myers, The exchange adsorption of ions from aqueous solutions by organic zeolites. II. Kinetics 1, *J. Am. Chem. Soc.* 69 (1947) 2836–2848.
- [66] P. SenthilKumar, S. Ramalingam, R.V. Abhinaya, S.D. Kirupha, T. Vidhyadevi, S. Sivanesan, Adsorption equilibrium, thermodynamics, kinetics, mechanism and process design of zinc(II) ions onto cashew nut shell, *Can. J. Chem. Eng.* 90 (2012) 973–982.